ADVANCED MATERIALS

DOI: 10.1002/adma.200601622

Semiconductor Sub-Micro-/Nanochannel Networks by Deterministic Layer Wrinkling**

By *Yongfeng Mei*,* *Dominic J. Thurmer*, *Francesca Cavallo*, *Suwit Kiravittaya*, and *Oliver G. Schmidt*

The wrinkling of thin films on substrate surfaces is a well-known phenomenon, and has been studied in different material systems in great detail for several decades.[1–11] While several potential applications of wrinkles have been put forward, such as applications in force spectroscopy in cells,[1] optical devices,[3] metrology methods,[9] and flexible electronics,[11] the use of wrinkles as complex nanochannel networks on a substrate surface to study nanofluidics[12–14] or to herald applications in bionanotechnology[15–17] seems an intriguing and almost obvious idea. Recently, the employment of folded thin films[18] with wrinkles that run perpendicular to the main fold has been suggested for realizing complex nanochannel systems,[4] but thus far fluid flow through such wrinkles has not been reported.

Here, we describe a technology that exploits the deterministic wrinkling and subsequent bond-back of a semiconductor layer to create well-defined and versatile nanochannel networks. The technology is termed "release and bond-back of layers" (REBOLA), and consists of the partial release, wrinkling, and bond-back of a compressively strained functional layer on a substrate surface. Linear and circular nanochannel networks, both of which consist of a main channel and several perpendicularly oriented branch channels, were fabricated by REBOLA. In these networks the periodicity and the positions of the branch channels could be tuned and controlled by changing the width of the partially released layers and by applying appropriate lithographic techniques. To elucidate the usefulness of REBOLA, we demonstrate nanofluidic transport as well as femtoliter filling and emptying of individual wrinkles on a standard semiconductor substrate.

The general concept of REBOLA is schematically outlined in Figure 1a.[19] A thin strained functional layer, deposited onto a sacrificial buffer layer, is partially released from the substrate surface by selectively etching away the sacrificial layer from one side. Once the strained functional layer is freed from the substrate, the strain elastically relaxes and causes wrinkles to form perpendicular to the etching front.[2a,20] Afterwards, the wrinkled functional layer bonds back to the substrate surface and forms a branched nanochannel network comprising the self-formed wrinkles, which connect to the main channel running along the edge of the back-

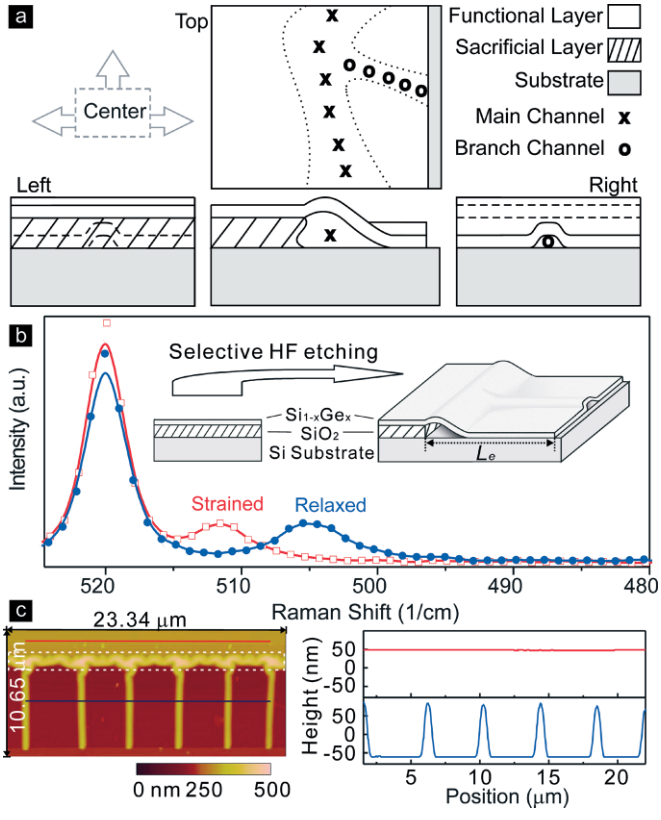

Figure 1. Fabrication and characterization of nanochannel networks by REBOLA. a) Generic description of the proposed micro-/nanochannel network. A single unit of such a network consists of a main channel and a perpendicularly oriented branch channel. b) Raman spectra of a strained and relaxed ultrathin $Si_{1-x}Ge_x$ film on a 100 nm thick SiO_2 layer. The inset shows a schematic illustration of the formation of the $Si_{1-x}Ge_x$ channel structure by HF etching of SiO_2. c) Atomic force microscopy (AFM) image of the linear network (left) and height profiles (right) along the lines indicated in the AFM image.

[*] Dr. Y. Mei, D. J. Thurmer, F. Cavallo, Dr. S. Kiravittaya, Prof. O. G. Schmidt
Max-Planck-Institut für Festkörperforschung
Heisenbergstrasse 1, 70569 Stuttgart (Germany)
E-mail: y.mei@fkf.mpg.de
Dr. Y. Mei, D. J. Thurmer, Prof. O. G. Schmidt
Institute for Integrative Nanosciences
IFW Dresden
Helmholtzstrasse 20, 01069 Dresden (Germany)

[**] We thank Dr. S. Mendach, Dr. C. Deneke, Dr. M. Stoffel, and Dr. A. Rastelli for helpful discussions, and U. Waizmann, A. Schulz, E. Coric, W. Winter, U. Zschieschang, and M. Riek for experimental assistance. We also thank Dr. Thamm at Karl Zeiss AG for use of the Axiocam HSm. This work is financially supported by the BMBF (03N8711). Supporting Information is available online from Wiley InterScience or from the author.

etched buffer layer. While Figure 1a represents a generic description of REBOLA that can be applied to many different material systems, geometries, and layer thicknesses, we concentrate in this Communication on semiconductor-based materials that are compatible with advanced Si and complementary metal oxide semiconductor (CMOS) technology. More precisely, we expose the surface of SiGe on SiO_2 on a Si (001) substrate to hydrofluoric acid. The acid gains access to the underlying SiO_2 through lithographically defined trenches, fine scratches, or defects in the SiGe layer and etches away the insulator material to a certain lateral distance (L_e). The compressively strained SiGe functional layer detaches from the substrate, wrinkles, and eventually forms into a branched nanochannel network by partially bonding back to the surface. A schematic 3D illustration of the final structure is given as an inset in Figure 1b.

We measured the change in strain in the $Si_{1-x}Ge_x$ layer before and after REBOLA by micro-Raman scattering, as presented in Figure 1b. The red curve represents the Raman spectrum of the strained SiGe layer before under-etching. The line at 520 cm^{-1} stems from the first-order longitudinal optical phonon Si–Si vibration mode of the Si substrate, whereas the peak at 512 cm^{-1} originates from the Si–Si vibration mode of the compressively strained SiGe layer. The blue spectrum is taken from an area where the SiGe layer was released and bonded back onto the Si substrate surface. The Si–Si vibration mode of this SiGe layer has been shifted by 7 cm^{-1} compared to the strained SiGe layer. Using the equation[21] $\omega_{Si} = 520 - 62x + \Delta_{Si}\Sigma$, we determine an average Ge composition of 24 % and a 1.1 % compressive strain in the $Si_{0.76}Ge_{0.24}$ film before etching.[22] The degree of relaxation can also be determined by measuring the increase in length of the wrinkled layer. An atomic force microscopy (AFM) image (left) and two line scans (right) are presented in Figure 1c: the red line scan was performed on the planar, pristine surface and the blue linescan on the wrinkled area. The integrated path (20.717 μm) across the wrinkled area is 1.187 % longer than the length of the line scan across the flat surface area (20.474 μm). Hence, the strain measurements obtained by micro-Raman spectroscopy and the line scan method agree reasonably well. The small difference may be attributable to the inhomogeneous strain across the thin SiGe film in the vertical direction, and/or the not perfectly equidistant positions of the branch channels.

REBOLA allows us to use standard lithography or simple mechanical scratching to define straight starting lines for the under-etching. Two examples of linear nanochannel networks are shown in Figure 2a. The network shown in the upper image of Figure 2a consists of a single-sided branched channel network directly connected to the main channel, which runs along the back-etched buffer layer. The middle image is a double-sided branched linear nanochannel network, with the main channel running in between the wrinkled branch channels.

A scanning electron microscopy (SEM) image, presented at the bottom of Figure 2a, reveals that the end of each branch channel, which is located at the starting edge, is open, and that the opening has an arc shape with a width of 300–500 nm and

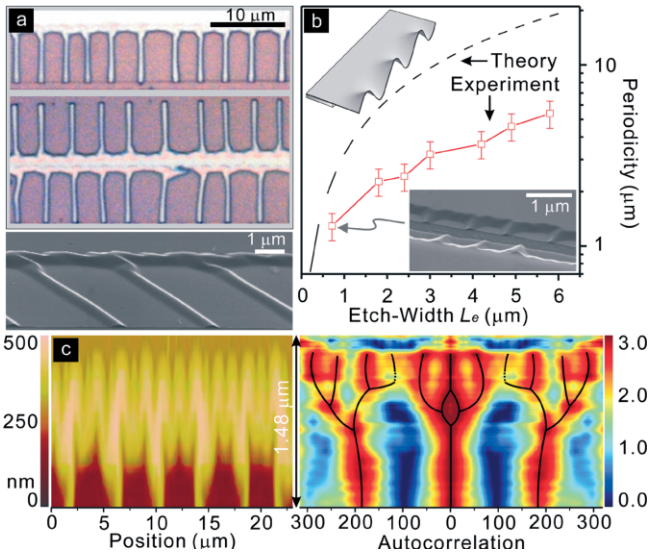

Figure 2. Experimental and theoretical analysis of linear nanochannel networks. a) Optical microscopy images of a linear nanochannel network with single-sided (upper) and double-sided branch channels (middle). A scanning electron microscopy (SEM) image of a single-sided linear nanochannel network is given in the lower panel. b) Periodicity of wrinkles as a function of etch width. The dashed curve shows a theoretical calculation for an entirely free-hanging wrinkled film (upper left inset). The lower right inset shows an SEM image of a nanochannel network, in which the height is about 40 nm and the width is about 150 nm. c) AFM image (left) of the linear network near the etching front (marked by the dashed white rectangle in Fig. 1c) and its autocorrelation pattern (right).

a height of ca. 120 nm (see also Supporting Information, Fig. S1). This SEM image confirms that the opposite branch channel ends are directly connected to the main channel that runs along the back-etched buffer layer. The average periodicity (λ_0) of the wrinkling (or the interdistance between two branch channels) parallel to the etching front is about 3.3 μm with a standard deviation of 17.1 %. As shown in Figure 2b, λ_0 increases with L_e in the experiment. A simple theoretical calculation based on minimization of the elastic energy of a free-hanging wrinkled film (Fig. 2b, upper left inset),[23] is used to fit the experimental result. We recognize that the periodicities predicted by theory show the same trend as the experiment, but the values are 2–3 times larger. This discrepancy is attributed to the interaction of the free-hanging film with the substrate once the wrinkling amplitude becomes larger than the thickness of the sacrificial layer. If the wrinkled film begins to partially bond back to the substrate surface, the layer cannot adapt its equilibrium periodicity as calculated for an entirely free hanging film, and λ_0 remains smaller than predicted by theory with increasing L_e. However, the film is not expected to tightly bond back to the surface during under-etching,[24] which signifies that λ_0 could still slightly increase. The SEM image shown in the lower right inset of Figure 2b reveals a nanochannel network composed of arc-shaped nanochannels with heights of ca. 40 nm and widths of ca. 150 nm. From this result, we confirm that the fabricated channels can be scaled down to several tens of nanometers.

ADVANCED MATERIALS

A detailed AFM investigation, shown in the left part of Figure 2c (also indicated in the left part of Fig. 1c by a white dashed rectangle), reveals that a complicated surface distortion of the SiGe film develops near the etching front. From top to bottom, Figure 2c shows that the periodicity of the wrinkling becomes larger but that the morphology remains similar, which is known as the "self-similar folding" phenomenon and is generally found near the boundary between a fixed and free layer (e.g., the etching front in our experiments).[25,26] The surface morphology of the SiGe film near the etching front was analyzed by an autocorrelation plot (right part of Fig. 2c), in which the maxima are marked as solid lines. The autocorrelation verifies that the periodicity of the wrinkles decreases towards the etching front, which has been explained previously by using the competition between stretching and bending in a layer at a fixed boundary.[25,26]

Customized linear nanochannel networks can be devised by mechanical scratching or lithography. We have also discovered that crystal defects in the film act as starting points for the under-etching, thereby producing circular nanochannel networks as shown in Figure S2. Well-defined holes, that is, circular patterns with diameters (d) ranging from 20 nm to several tens of micrometers were fabricated by photo- and electron-beam lithography. We use these structures to understand the influence of the channel diameter (D) on the number of branch channels in the circular networks. Applying an identical etch-width ($L_e = 2.5$ μm) to all circular patterns, a statistical analysis of the number of branch channels m as a function of the diameter D ($D = d + 2L_e$) was carried out as shown in Figure 3a (blue circles). The inset presents an optical microscopy image of an array of circular networks created by REBOLA.

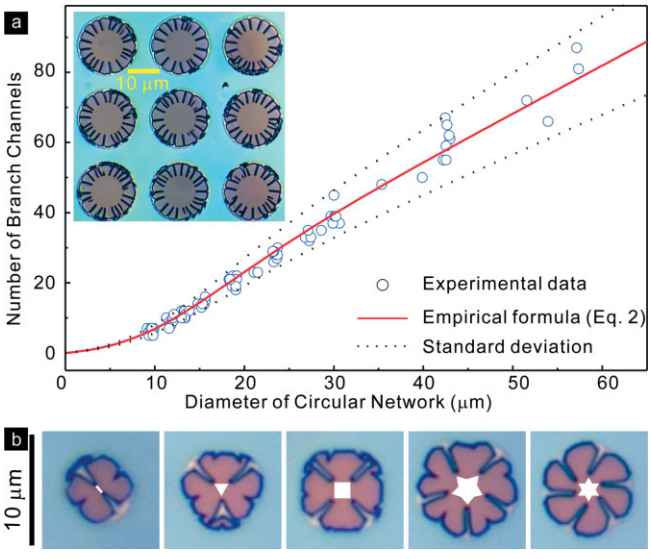

Figure 3. Size and shape effects on circular nanochannel networks. a) Number of branch channels versus diameter of circular network. Inset shows array of circular networks. b) Optical images of circular networks with 2–6 well-positioned branch channels. The circular networks evolve from a lithographically defined initial pattern. (Defined pattern shapes form left to right: short line, triangle, square, and five- and six-pointed stars.)

The average periodicity of the branch channels in the circular network (which is calculated from the perimeter of the etching front divided by the number of branch channels) approaches λ_0, when the diameter tends to infinity and the circular becomes a linear network. In our study we find that the periodicity λ of the branch channels as a function of D can be phenomenologically fitted by the exponential decay function

$$\lambda = \lambda_0 + A \exp(-D/D_c) \quad (1)$$

where A is the amplitude of periodicity decaying and D_c is the critical diameter. Using the relation $m\lambda = \pi D$ for circular networks, m as a function of D can be expressed as

$$m = \frac{\pi D}{\lambda_0 + A \cdot \exp(-D/D_c)} \quad (2)$$

For a good fit of our data in Figure 3a (red line), we obtain $\lambda_0 = 2.30$ μm, $A = 12$ μm and $D_c = 6$ μm, respectively. Here, λ_0 corresponds to the average periodicity of a circular network with infinite diameter, and agrees well with the experimental value of 2.3 μm found for the corresponding linear network. The standard deviation of λ_0 from linear networks (17.1 %) is introduced into our fit and explains the fluctuation of branch channel numbers in Figure 3a. When D drops below D_c, it is not possible to solve the number of branch channels with Equation 2 because D is comparable to or smaller than $2L_e$. To exert control over the position and number of branch channels in circular networks with diameters of around D_c, well-defined initial patterns (indicated as white boxes in Fig. 3b) with special shapes were designed, such as short lines, triangles, squares, and five- and six-pointed stars. In these cases, the formation of the channels is initiated by the corners of each shape, and well-positioned concentric branches are obtained in Figure 3b.

One potential application of these nanochannel networks is their use in nanofluidics. Our proof-of-concept incorporates fluid transfer behavior in a linear channel network and several individual wrinkles (Fig. S3), which have been prewetted with the applied fluid (ethylene glycol with 3.29×10^{-4} M rhodamine 6G). Fluid droplets of femtoliter volumes, created by a self-made drop generator, were introduced into this network, as illustrated by a video microscopy frame in the left part of Figure 4a (the entire video of fluid flow is available as Supporting Information). The right part of Figure 4a is a schematic diagram of the droplet generator, which is based on the principle of thermal expansion of vapor bubbles in a glass capillary by heating the inserted thermal conductor metal wire (see details in Experimental). The video microscopy documents the fluid flow through the linear nanochannel network, and the selected filling and emptying of a large wrinkle found in the lower left corner of Figure 4a (marked by a yellow dashed rectangle). Such a stand-alone wrinkle was previously referred to as a "blister".[2b] The filling is driven by corner flow through the linear network, which is caused by dissimilar chemical potentials of the fluid in the different channels.[27]

A time of 250 ms was needed for the fluid to flow from the position of the applied droplet to the large wrinkle. Selected chronological video frames, concentrating on the filling and

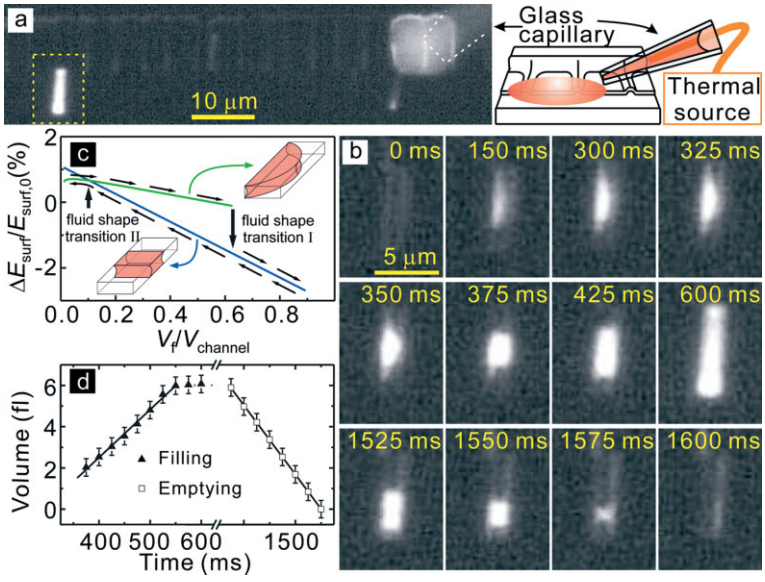

Figure 4. Femtoliter-scale fluidics within linear nanochannel networks. a) Selected video frame (left) of liquid transport through a linear nanochannel network, and a schematic diagram (right) of the experimental setup used to generate droplets. b) A series of selected video frames highlighting the transport behavior of fluid in the large wrinkle. c) Surface energy as a function of fluid volume, in which the green line represents the arc-shaped fluid (upper right inset) and the blue line describes the rectangular-shaped fluid model (lower left inset). d) Volume of fluid inside the wrinkle as a function of time.

emptying process of the large wrinkle, are given in Figure 4b. The small branch channel of the upper linear network is situated at the very left side of the large wrinkle thus ensuring controlled fluid injection into the left part of the large wrinkle. The first frame at 0 ms was taken directly before filling of the large wrinkle started. From 0 to 350 ms, arc-like shapes of the fluid are observed in the large wrinkle. From 375 to 1575 ms, rectangular shapes are formed during fluid filling and subsequent emptying. In last frame (1600 ms), the arc shape appears again on the other side of the large wrinkle.

To understand the observed fluid shape transitions during the fluid filling and emptying, we consider a simplified geometry, which is sufficient to capture the main phenomena of our observations. The large wrinkle is modeled as a rectangular container with a volume $V_{channel}$, and the total surface energy E_{surf} is calculated.[28] Two different fluid shapes, which are given by the Young–Laplace relation,[27,29] are considered (see insets of Fig. 4c). The change in surface energy as the channel fills and empties is shown in Figure 4c. For shape 1 (upper right inset), the fluid is confined to one of the container walls while shape 2 (lower left inset) represents a squarelike fluid plug that extends from one wall to the other. In the very beginning (up to a relative volume of 0.04), the fluid is forced to the left edge, and E_{surf} increases because of the increase of surface area. Then, E_{surf} gradually decreases as the fluid volume V_f increases because of the hydrophilic nature of the fluid. In this volume regime, the fluid shape 2 experiences a lower surface energy than does shape 1. However, the fluid cannot change from shape 1 to shape 2, because it has not yet reached the opposite wall. Once the fluid reaches the opposite wall (which occurs for a normalized volume of 0.63), a rapid fluid shape transition occurs ("fluid shape transition I"). Continuous fluid supply into the channel keeps filling the channel. For emptying, we can use the same diagram as for filling. In this case, the fluid remains in shape 2 until a very small volume is occupied (normalized volume 0.10). For this volume, the surface energies cross and the fluid plug changes its shape to the one confined to the left wall ("fluid shape transition II") until the channel is completely emptied.

Figure 4d shows the measured fluid volume as a function of time. After complete filling at a constant flow rate of 23.2 fL s^{-1} from 375 to 600 ms, the large wrinkle empties with a constant slightly higher flow rate of 33.5 fL s^{-1} (from 1425 to 1600 ms). We note that the emptying process coincides with the almost complete evaporation of the generated droplet, which reverses the pressure conditions within the nanochannel network and drives the emptying of the large wrinkle.

Our studies suggests that an individual wrinkle might act as a good container for fluids of femtoliter volume, while the branch channels in the network represent an efficient fluid supplier or injector on the nanometer scale. The experiments also demonstrate that small branch channels can deliberately be used to fill-up larger channels, which enables REBOLA to up-scale and in principle connect the nanochannel networks to the macroscopic world. We believe that the corner flow in such nanochannels may become increasingly important and interesting in nanofluidics because of its unique properties, such as enhanced flow,[30] droplet generation within linear channels,[31] and fluid mixing in networks.[32] REBOLA combines a bottom-up process—the wrinkling of a layer—with refined but standard main-stream semiconductor technology (top-down process), and is thus expected to stimulate plenty of basic studies as well as various on-chip integrative applications.

Finally, we point out several advantages of REBOLA over other existing techniques: The size of the REBOLA channels is easily scalable by precisely engineering strain and thickness of the wrinkling layer as well as the under-etching length. Refined and expensive tools, such as electron-beam or extended UV lithography, are not necessarily required to fabricate nanometer-sized wrinkles. The technique is compatible with advanced Si and CMOS technology. Furthermore, the top wrinkling layer is a single crystalline semiconductor layer and can easily be made optically or electronically active. This property might be beneficial to read out information stored in the fluid or to study interactions between the active semiconductor layer and the fluid.

In summary, we have demonstrated a technology (REBOLA) that exploits the deterministic wrinkling of a semiconductor layer to create well-defined and versatile nanochannel

ADVANCED MATERIALS

networks. In linear networks, the periodicity of branch channels as a function of etch width was analyzed and compared with theoretical calculations. A self-similar folding phenomenon of wrinkles near a fixed boundary was revealed by autocorrelation analysis. The formation of branch channels within circular networks was studied on different length scales and was controlled by the size of the etched circular network and the shape of the initial pattern. To elucidate the usefulness of REBOLA, we exemplified nanofluidic transport as well as femtoliter filling and emptying of individual wrinkles on a standard semiconductor substrate, in which corner flow played an important role.

Experimental

Fabrication of Nanochannel Networks: Ultrathin silicon on insulator (SOI) wafers with a 27 nm top Si layer on 100 nm SiO_2 were loaded into an ultrahigh vacuum molecular beam epitaxy (UHV–MBE) system. A 40 nm layer of $Si_{1-x}Ge_x$ with a uniform Ge composition of 8 % was pseudomorphically grown on the ultrathin SOI substrates at 350 °C. After growth, the SiGe/SOI structures were oxidized in a tube furnace at 900 °C for 100 min in ambient oxygen. The dry oxidation was followed by a 2 h post-annealing step performed in ambient nitrogen. The grown SiO_2 layer was then removed by wet-chemical etching using a dilute HF acid solution. After defining the starting edge by mechanical scratching, or lithography followed by reactive ion etching (RIE), a 49 % HF solution was used to selectively remove the buried SiO_2 layer, resulting in the formation of nanochannel networks along the designed edges or patterns. Generally, we defined long narrow lines by photo- or electron-beam lithography (with widths varying from 50 nm to several micrometers) for the single-sided, linear branched channel networks, while two such lines with a tunable interdistance were carefully designed to connect two single-sided branched channel networks to form a double-sided branched channel network. The etching distance was easily controlled by the duration of HF etching.

Fluidics Setup: Observing the fluidic behavior in the channel networks was accomplished by a Zeiss Axioskop upright microscope connected to an AxioCam MR for general optical color images, and an AxioCam HSm for high-speed (60–198 frames s^{-1}) black&white videos. A rhodamine 6G specific fluorescence filter set was used to visualize the fluid transport behavior. The glass capillaries (2–10 μm diameter tip) were maneuvered by using a PI NanoCube piezoelectric XYZ positioning stage mounted on a larger PI optics translation stage. With this combination, a positioning accuracy of below 1 μm over a distance of 15 mm was achieved.

Solutions of rhodamine 6G in various solvents were created using a particulate lambdachrome rhodamine powder from Lambda Physik. Solvents used included ethanol, ethylene glycol, and deionized water. Concentrations of 5×10^{-6} M for ethanol, 3.29×10^{-4} M for ethylene glycol, and 4.14×10^{-4} M for water were used.

The femtoliter generator, shown in the right part of Figure 4a, was self-made and was based on the principle of thermal expansion of bubbles in the glass capillary. A metal wire (polymer-insulated copper, 0.4 mm in diameter) was used as a thermal conductor connected to the thermal source (thermal iron) and immersed in the fluid (ethylene glycol with 3.29×10^{-4} M dye) in the glass capillary to heat the vapor bubbles. Heating the metal wire for a short time (several seconds) caused the bubbles in the capillary to expand, creating a pressure inside the capillary. This generated a fluid droplet of femtoliter volume.

Received: July 19, 2006
Revised: December 7, 2006
Published online: July 12, 2007

[1] A. K. Harris, P. Wild, D. Stopak, *Science* **1980**, *208*, 177.
[2] a) T.-Y. Zhang, X. Zhang, Y. Zohar, *J. Micromech. Microeng.* **1998**, *8*, 243. b) X. Zhang, Y. Zohar, T.-Y. Zhang, *Microelectromech. Syst.* **1998**, *66*, 379.
[3] N. Bowden, S. Brittain, A. G. Evans, J. W. Hutchinson, G. M. Whitesides, *Nature* **1998**, *393*, 146.
[4] O. G. Schmidt, N. Schmarje, C. Deneke, C. Muller, N. Y. Jin-Phillipp, *Adv. Mater.* **2001**, *13*, 756.
[5] E. Cerda, K. Ravi-Chandar, L. Mahadevan, *Nature* **2002**, *419*, 579.
[6] V. Ya. Prinz, *Microelectron. Eng.* **2003**, *69*, 466.
[7] E. Cerda, L. Mahadevan, *Phys. Rev. Lett.* **2003**, *90*, 074 302.
[8] P. J. Yoo, H. H. Lee, *Phys. Rev. Lett.* **2003**, *91*, 154 502.
[9] C. M. Stafford, C. Harrison, K. L. Beers, A. Karim, E. J. Amis, M. R. Vanlandingham, H.-C. Kim, W. Volksen, R. D. Miller, E. E. Simonyi, *Nat. Mater.* **2004**, *3*, 545.
[10] K. Efimenko, M. Rackaitis, E. Manias, A. Vaziri, L. Mahadevan, J. Genzer, *Nat. Mater.* **2005**, *4*, 293.
[11] D.-Y. Khang, H. Jiang, Y. Huang, J. A. Rogers, *Science* **2006**, *311*, 208.
[12] T. M. Squires, S. R. Quake, *Rev. Mod. Phys.* **2005**, *77*, 977.
[13] J. C. T. Eijkel, A. van den Berg, *Microfluid. Nanofluid.* **2005**, *1*, 249.
[14] P. J. A. Kenis, A. D. Stroock, *MRS Bull.* **2006**, *31*, 87.
[15] M. A. Northrup, *Nat. Mater.* **2004**, *3*, 282.
[16] J. W. Hong, V. Studer, G. Hang, W. F. Anderson, S. R. Quake, *Nat. Biotechnol.* **2004**, *22*, 435.
[17] P. S. Dittrich, A. Manz, *Nat. Rev. Drug Discovery* **2006**, *5*, 210.
[18] O. G. Schmidt, K. Eberl, *Nature* **2001**, *410*, 168.
[19] O. G. Schmidt, Y. Mei, D. Thurmer, F. Cavallo, *European Patent Application 06001885.0* **2006**.
[20] A. I. Fedorchenko, A.-B. Wang, V. I. Mashanov, H.-H. Cheng, *J. Mech.* **2005**, *21*, 131.
[21] J. C. Tsang, P. M. Mooney, F. Dacol, J. O. Chu, *J. Appl. Phys.* **1994**, *75*, 8098.
[22] x is the Ge composition, Δ_{Si} the Raman shift normalized by $x=1$ (i.e., assuming 100 % composition of Ge in the SiGe layer), and Σ is the normalized strain of the measured film using the mismatch strain 0.0417 (i.e., the strain between pure Ge and pure Si making $\Sigma = 1$ for pure Ge grown epitaxially on Si (001)).
[23] A more detailed calculation will be published elsewhere.
[24] G. M. Cohen, P. M. Mooney, V. K. Paruchuri, H. J. Hovel, *Appl. Phys. Lett.* **2005**, *86*, 251 902.
[25] S. Conti, A. DeSimone, S. Müller, *Comput. Methods Appl. Mech. Eng.* **2005**, *194*, 2534.
[26] E. Cerda, L. Mahadevan, J. M. Pasini, *Proc. Natl. Acad. Sci. USA* **2006**, *101*, 1806.
[27] J. C. T. Eijkel, A. van den Berg, *Lab Chip* **2005**, *5*, 1202.
[28] E_{surf} is calculated by $E_{surf} = \gamma_{sf}A_{sf} + \gamma_{fv}A_{fv} + \gamma_{sv}A_{sv}$ where, s, f, and v denote solid, fluid, and vapor phase, respectively; γ_{ij} is the surface tension between phase i and j; A_{ij} is the surface area between phase i and j. The surface energy without any fluid is $E_{surf,0} = \gamma_{sv}A_{sv}$, while the relative surface energy $\Delta E_{surf}/E_{surf,0} = (E_{surf} - E_{surf,0})/E_{surf,0}$ is considered. The simplified channel geometry is 1.7 μm wide, 470 nm high, and 7.5 μm long.
[29] N. R. Tas, P. Mela, T. Kramer, J. W. Berenschot, A. van den Berg, *Nano Lett.* **2003**, *3*, 1537.
[30] J. C. T. Eijkel, B. Dan, H. W. Reemeijer, D. C. Hermes, J. G. Bomer, A. van den Berg, *Phys. Rev. Lett.* **2005**, *95*, 256 107.
[31] P. Garstecki, M. J. Fuerstman, H. A. Stone, G. M. Whitesides, *Lab Chip* **2006**, *6*, 437.
[32] D. Belder, M. Ludwig, L. W. Wang, M. T. Reetz, *Angew. Chem. Int. Ed.* **2006**, *45*, 2463.

